Journal of Rajasthan Academy of Physical Sciences
ISSN: 0972-6306; URL: http://raops.org.in
Vol.25, No.1&2, January-June, 2026, 42-65

UNSTEADY THERMAL TRANSPORT IN ELASTICO-VISCOUS CASSON FLUID FLOW OVER AN ALIGNED FLAT PLATE WITH LEADING-EDGE ACCRETION AND SLIP EFFECTS

Bikash Koli Saha[1] and **Anuja Sinha**[2]
[1&2]Independent Researcher, Mathematics, Guwahati, Kamrup Metropolitan, Assam-781018, India
Email: bikashkoli100@gmail.com

Abstract : A detailed analytical–numerical study is performed to examine the coupled heat and mass transfer behavior of an elastico-viscous fluid interacting with a Casson fluid over an aligned flat plate experiencing leading-edge accretion. The fundamental conservation equations governing the flow are reduced to a similarity framework through the Blasius–Rayleigh–Stokes transformation combined with Walter's Liquid Model B′ formulation. This procedure converts the original partial differential system into a set of strongly nonlinear coupled ordinary differential equations. The transformed boundary value problem including modified slip boundary conditions, are then resolved numerically via MATLAB's bvp4c solver. The analysis reveals that elastico-viscous parameters significantly influence the momentum distribution and substantially alter the boundary layer structure. Parametric analyses are carried out to examine the velocity, temperature and concentration fields, providing deeper physical insight into the transport mechanisms. The results indicate a pronounced reduction in temperature and concentration distributions accompanied by a significant thinning of the thermal and solutal boundary layers. Although the velocity profile initially exhibits parameter-dependent variation, it ultimately decreases and attains a stabilized momentum boundary layer thickness. Overall, enhanced convective transport combined with diminished near-wall diffusion leads to reduced thermal and solutal fields, while elastico-viscous resistance contributes to the stabilization of momentum transfer.

Keywords : Aligned Flat Plate, Leading Edge Accretion, Casson Fluid, Elastico-Viscous Fluid, Slip Boundary Conditions

1. Introduction

The growing global demand for steel, driven by its widespread use in construction, infrastructure, and manufacturing, underscores the energy-intensive nature of its production from coal and iron ore. Rolling a fundamental forming operation in steel processing is extensively applied in industries such as aerospace and fluid transport and is categorized into hot and cold processes based on temperature. Accurate thermal

regulation during rolling is essential to maintain product integrity, minimize equipment degradation and ensure reliable, cost-efficient mill performance.

Sheikholeslami and Ganji [25] numerically examined transient magnetohydrodynamic nanofluid flow incorporating thermal radiation effects to explicate their combined influence on heat transfer characteristics. Khan and Khan [15] conducted an in depth analysis of magnetohydrodynamic boundary-layer flow in a power-law nanofluid introducing an innovative mass flux boundary constraint to systematically investigate its effects on momentum distribution and concentration transport dynamics. Sravan and Rushi [28] conducted a detailed investigation into the unsteady magnetohydrodynamic free-convective flow of a nanofluid past a vertically moving plate, elucidating its influence on boundary layer evolution and the associated heat transfer mechanisms.

Shamshuddin et al. [24] conducted a numerical investigation of viscous flow and thermal transport between dual rotating stretchable disks incorporating a non-Fourier heat flux framework to capture finite speed thermal propagation effects. Sravan and Rushi [27] analytically explored the impact of coupled homogeneous–heterogeneous chemical reactions on magnetohydrodynamic stagnation-point nanofluid flow over a cylindrical surface incorporating the influence of a spatially varying internal heat source/sink to expound complex thermal reactive transport behavior. Dianchen Lu et al. [9] presented a comprehensive investigation of unsteady nanofluid flow and thermal transport characteristics by employing the Blasius Rayleigh Stokes variable to interpret transient boundary layer behavior.

Reddy et al. [22] performed an extensive investigation employing a non-Fourier heat conduction framework that incorporates thermal relaxation time, thereby addressing and overcoming the inherent limitations associated with the classical Fourier heat conduction law. Ali et al. [4] examined the combined influence of Stefan blowing, thermal radiation and the Cattaneo–Christov heat flux model on nanofluid flow embedded with motile microorganisms, specifically under leading edge ablation and accretion conditions. Kumar et al. [16] along with Mabood and Khan [17] examined laminar Rayleigh Stokes and Blasius boundary layer flows in the presence of ohmic (Joule) heating. Their analyses demonstrated that variations in governing physical parameters significantly influence both momentum and heat transfer behavior, highlighting the potential to optimize thermal management strategies in diverse engineering systems.

Oladimeji et al. [21] analyze nanofluid convection using the Blasius Rayleigh Stokes model with boundary velocity slip. By formulating and solving the governing equations, they assess how slip parameters and nanoparticle presence influence flow structure and thermal transport. Their findings clarify boundary layer behavior and highlight the critical role of slip effects in regulating and improving nanofluid heat transfer.

Adebayo et al. [1], Ishaq and Ahmad [12] as well as Al Nuwairan and Souayeh [2] utilized the Blasius Rayleigh Stokes transformation incorporating slip boundary conditions to analyze the transient convective flow behavior of nanofluids. Furthermore, Gangadhar et al. [11] investigated the forced convective boundary layer dynamics

involving gyrotactic microorganisms by implementing a hybrid numerical scheme that integrates collocation techniques with finite difference methods. Leading-edge accretion may induce convective and unstable acceleration, thereby altering flow behavior and influencing heat transfer performance across various systems. Animasaun et al. [5] analyzed ternary hybrid nanofluid flow over horizontal surfaces and showed that such acceleration mechanisms significantly modify thermal characteristics and enhance heat transfer efficiency in engineering processes.

Wang et al. [30] systematically investigated the influence of nanoparticle concentration on the thermal characteristics of water based nanofluids. Their analysis emphasized particle aggregation mechanisms and demonstrated the enhancement of heat transfer performance in nanofluid systems. Vaidya et al. [29] applied Blasius Rayleigh Stokes transformations to examine how heat transfer characteristics influence unsteady flow over a moving plate. They found that increasing the dimensionless reference temperature and modifying slot parameters reduces the nanofluid's thermal conductivity. Oladapo et al. [20] examined radiative effects on Casson fluid flow along an inclined plane, inspired by applications in solar powered aircraft technology, employing the Blasius Rayleigh Stokes transformation to characterize the governing flow dynamics under the prescribed conditions.

Alammari [3] and Nandi et al. [19] analyzed the flow of Casson nanoliquids within a stretching channel, emphasizing the application of particle swarm optimization (PSO) to enhance numerical stability and optimize flow performance in complex industrial systems. Their work also explored three dimensional steady nanofluid flow, incorporating nonlinear thermal radiation and binary chemical reaction effects. Emphasizing the reduction of leading-edge deposition and the enhancement of thermal performance, Jayaprakash et al. [13] explored the implementation of Casson fluid models in cooling mechanisms used in rolling mills and heat exchanger systems. In a related investigation, Jayaprakash and Govindan [14] examined Casson based nanofluids incorporating diffusion and chemical reaction effects during accretion processes, thereby advancing the design of durable and high-performance materials suitable for elevated temperature conditions. Eswaramoorthi et al. [10] numerically investigated rotating CNT nanofluid flow incorporating thermal radiation, Joule heating and autocatalytic reactions to clarify coupled thermal chemical effects in complex nanofluid systems.

Yahaya et al. [31] examine heat transfer enhancement in oblique stagnation point flow of a hybrid nanofluid over a permeable contracting surface. Using Response Surface Methodology (RSM), the study optimizes key physical parameters to improve thermal performance and fluid flow characteristics providing useful insights for advanced cooling and thermal management systems. Asghar et al. [7] numerically examined MHD Casson hybrid nanofluid flow over a permeable stretching/shrinking surface within a porous medium incorporating Joule heating to assess its impact on velocity and temperature fields. Their findings emphasize the combined influence of non-Newtonian rheology,

magnetic interaction and porous drag on thermal performance enhancement. Saha [23] systematically explores the dynamics of elastico–viscous boundary layer flow over a wedge configuration, integrating nanofluid interaction mechanisms to elucidate their influence on momentum transport and thermal characteristics.

Existing studies highlight the growing significance of non-Newtonian nanofluids in enhancing thermal performance, evolving from simple nanoparticle based conductivity enhancement to advanced shear-dependent and coupled heat mass transfer models suited for high temperature and magnetized systems. This study examines the unsteady flow of an elastico-viscous Casson nanofluid flow induced by a horizontally stretching surface with a translating slot, incorporating multiple slip conditions and oscillatory boundary effects within Buongiorno's framework. The effects of Brownian motion, thermophoresis, Prandtl and Lewis numbers and thermal and solutal Grashof numbers are systematically evaluated, providing a comprehensive analysis of the resulting velocity, temperature and concentration distributions.

2. Mathematical Formulation

An unsteady two-dimensional laminar flow of an incompressible elastico-viscous Casson fluid is considered over a semi-infinite flat plate (x ≥ 0) incorporating a translating slot. The velocity components in the x and y directions are $u(x,y,t)$ and $v(x,y,t)$, while $T(x,y,t)$ and $C(x,y,t)$ denote the temperature and concentration fields with ambient states T_∞ and C_∞. The physical model is depicted in Fig. 2.1. Inspired by the analyses of Song et al. [26] and Cao et al. [8], Buongiorno's nanofluid model is adapted to incorporate thermophoresis and Brownian diffusion driven by concentration gradients.

The constitutive modeling is essentially a hybrid between Casson plasticity and elastico-viscous type of Walters' liquid model B'.

$$\tau_{ij} = \begin{cases} \left(\mu_B + \frac{p_y}{\sqrt{2\pi}}\right) 2e_{ij}, \pi > \pi_c \\ no\ flow, \qquad \pi \leq \pi_c \end{cases}$$

For elastico-viscous fluids, the extra stress tensor is

$$\tau_{ij} = -p\delta_{ij} + 2\mu e_{ij} - k_0 \frac{D}{Dt} e_{ij}$$

To construct our required model, replace the Newtonian viscosity in Walters' liquid B' with Casson effective viscosity:

$\tau_{ij} = -p\delta_{ij} + 2\mu_B\left(1 + \frac{1}{\beta}\right) e_{ij} - k_0 \frac{D}{Dt} e_{ij}$, τ_{ij} is the stress tensor, p the pressure, δ_{ij} the Kronecker delta, μ_B the plastic viscosity, β the Casson parameter, e_{ij} the strain-rate tensor, k_0 the elastico-viscous parameter, and $\frac{D}{Dt}$ the material derivative.

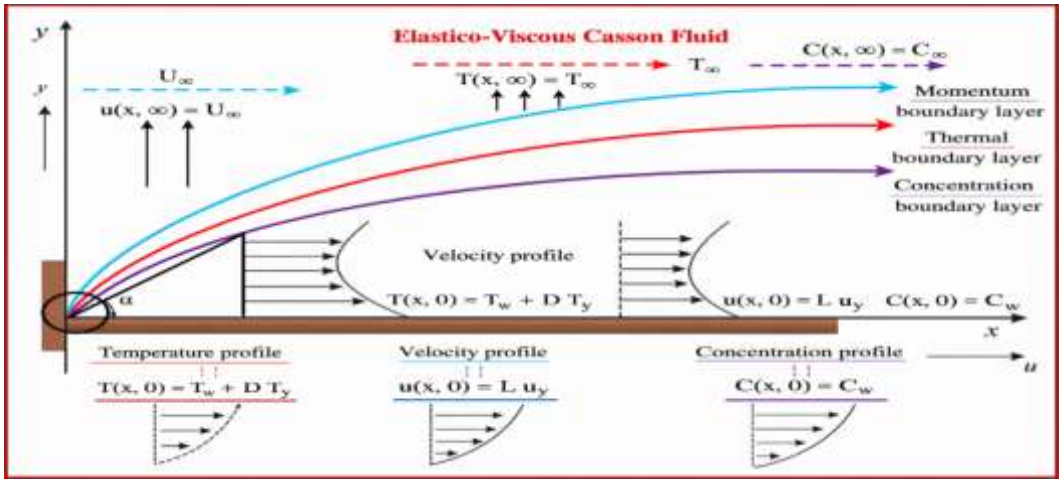

Fig. 2.1 : Physical Model of the Flow

The governing framework follows the formulation established by Dianchen *et al.* [9].

$$\frac{\partial u}{\partial x}+\frac{\partial v}{\partial y}=0 \tag{1}$$

$$\frac{\partial u}{\partial t}+u\frac{\partial u}{\partial x}+v\frac{\partial u}{\partial y}=\upsilon\left(1+\frac{1}{\beta}\right)\frac{\partial^2 u}{\partial y^2}+g\beta_c(C-C_\infty)+g\beta_T(T-T_\infty)-\frac{k_0}{\rho}\left[\frac{\partial}{\partial t}\left(\frac{\partial^2 u}{\partial y^2}\right)+u\frac{\partial^3 u}{\partial x\,\partial y^2}+v\frac{\partial^3 u}{\partial y^3}-\frac{\partial u}{\partial y}\frac{\partial^2 u}{\partial x\,\partial y}-\frac{\partial v}{\partial y}\frac{\partial^2 u}{\partial y^2}\right]=0 \tag{2}$$

$$\frac{\partial T}{\partial t}+u\frac{\partial T}{\partial x}+v\frac{\partial T}{\partial y}=\sigma\frac{\partial^2 T}{\partial y^2}+\varepsilon\left[D_B\frac{\partial T}{\partial y}\frac{\partial C}{\partial y}+\left(\frac{D_T}{T_\infty}\right)\left(\frac{\partial T}{\partial y}\right)^2\right] \tag{3}$$

$$\frac{\partial C}{\partial t}+u\frac{\partial C}{\partial x}+v\frac{\partial C}{\partial y}=D_B\frac{\partial^2 C}{\partial y^2}+\left(\frac{D_T}{T_\infty}\right)\frac{\partial^2 T}{\partial y^2} \tag{4}$$

Here, υ kinematic viscosity, β and k_0 represents the Casson and elastico-viscous parameter governing nonlinear rheological effects, g is the gravitational acceleration, β_C and β_T correspond to the solutal and thermal expansion coefficients, ρ is the fluid density, σ indicates thermal diffusivity, ε is the heat capacity ratio, D_T and D_B denote the thermophoretic and Brownian diffusion coefficients, respectively.

The corresponding boundary constraints are formulated as follows:

$$u(y)=L\frac{\partial u}{\partial y},\ v(y)=0,\ C(y)=C_W,\ T(y)=T_W+D\frac{\partial T}{\partial y}\ \text{at}\ y=0 \tag{5}$$

$$u(y)=0,\ C(y)=C_\infty,\ T(y)=T_\infty\ \text{at}\ y\to\infty \tag{6}$$

At $y=0$, the streamwise velocity satisfies a linear slip condition, such that the wall velocity U_w is proportional to the shear rate, i.e., $u(y)=U_w\propto\frac{\partial u}{\partial y}=L\frac{\partial u}{\partial y}\Big\}_{y=0}=0$, where L denotes the slip coefficient. The normal velocity vanishes at the surface,

indicating no penetration. The thermal and concentration fields at the wall obey gradient-based conditions, expressed as $T = T_W + D\frac{\partial T}{\partial y}$ and $C = C_w$, where D is the thermal slip parameter and C_w is a prescribed constant. As $\rightarrow \infty$, the flow asymptotically approaches quiescent ambient conditions, $u \rightarrow 0,\ T \rightarrow T_\infty$, and $C \rightarrow C_\infty$, representing a stagnant far-field with uniform temperature and concentration.

By employing the Blasius–Rayleigh–Stokes similarity transformation, the governing equations are reformulated through an appropriately defined stream function representation.

$$\zeta = \frac{y}{\sqrt{vtcos\alpha + \frac{vx}{U_w}sin\alpha}};\quad \psi = U_w\sqrt{vtcos\alpha + \frac{vx}{U_w}sin\alpha}\, f(\zeta); T(x,y,t) = T_\infty + \theta(\zeta)(T_W - T_\infty);$$

$$C(x,y,t) = C_\infty + \phi(\zeta)(C_W - C_\infty) \tag{7}$$

In this formulation, ζ represents the similarity variable employed to reduce the governing equations, ψ denotes the stream function characterizing the flow field, U_w denotes the stretching velocity of the sheet, v is the kinematic viscosity, α represents the inclination angle, and $f(\zeta)$ is the dimensionless similarity function, where the composite length scale $\sqrt{vtcos\alpha + \frac{vx}{U_w}sin\alpha}$ accounts for both temporal and spatial diffusion effects, $T(x,y,t)$ specifies the fluid temperature distribution and $C(x,y,t)$ describes the corresponding concentration profile.

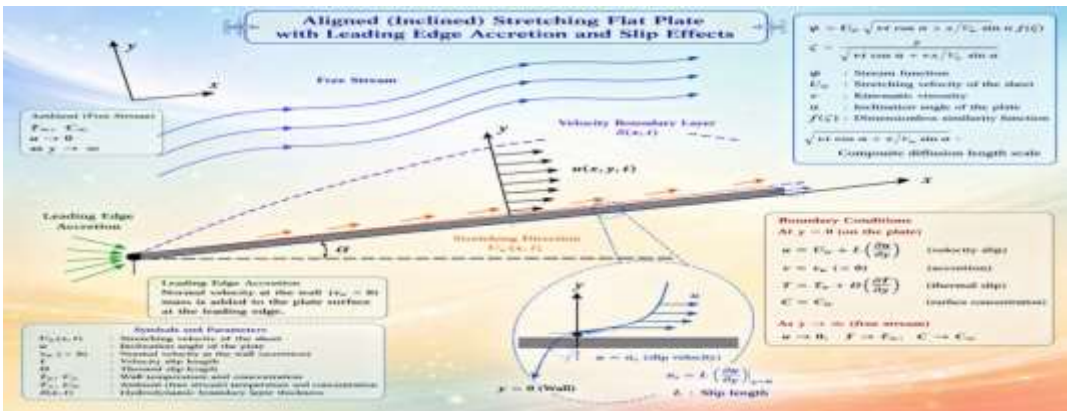

Fig. 2.2 : Physical Model of Stretching Sheet

The flow is considered over an inclined stretching flat plate, where the leading-edge accretion is modeled through a composite spatio-temporal diffusion scale, while velocity and thermal slip conditions are imposed at the surface to capture non-classical interfacial effects. This coupling reflects a leading-edge accretion mechanism, where the boundary layer thickness evolves due to both time-dependent diffusion and stream-wise stretching effects is shown in fig 2.2.

By invoking relation (7), the coupled governing equations subject to boundary constraints (1) – (6) are systematically transformed into a set of nonlinear ordinary differential equations expressed as follows:

$(1+\beta)f'''(\zeta) + \frac{\beta}{2} f''(\zeta)\{\cos\alpha\zeta+\sin\alpha\, f(\zeta)\} - Gr\theta - Gm\phi +$

$k_1\beta\,[\,\cos\alpha\{f'''(\zeta)+\frac{\zeta}{2}\, f'^{v}(\zeta)\} + \mathrm{Sin}\alpha\{f'(\zeta)\, f'''(\zeta) + \frac{f(\zeta)}{2} - \frac{f''(\zeta)}{2} + \frac{\zeta}{2} f''(\zeta)\, f'''(\zeta)] = 0$ (8)

$\theta''(\zeta) + \frac{Pr}{2}\{\cos\alpha\zeta+ \sin\alpha\, f(\zeta)\}\, \theta'(\zeta) + \{\theta'(\zeta)\}^2 N_t + \theta'(\zeta)\, \phi'(\zeta)\, N_b = 0$ (9)

$\phi''(\zeta) + \frac{Le}{2}\{\cos\alpha\zeta+ \sin\alpha\, f(\zeta)\}\, \phi'(\zeta) + \theta''(\zeta)\frac{N_t}{N_b} = 0$ (10)

Where Gr = $\frac{g\beta_T((T_W-T_\infty)(\upsilon t\cos\alpha+\frac{\upsilon x}{U_w}\sin\alpha)}{\upsilon U_w}$; Gm = $\frac{g\beta_C((C_W-C_\infty)(\upsilon t\cos\alpha+\frac{\upsilon x}{U_w}\sin\alpha)}{\upsilon U_w}$; k_1 = $\frac{k_0}{\rho(\upsilon t\cos\alpha+\frac{\upsilon x}{U_w}\sin\alpha)}$; $Le = \frac{\upsilon}{D_B}$; $\mathrm{Pr} = \frac{\upsilon}{\sigma}$; $N_t = \frac{\varepsilon D_T(T_w-T_\infty)}{\sigma T_\infty}$ and $N_b = \frac{\varepsilon D_B(C_w-C_\infty)}{\sigma}$ are the thermal Grasof number, mass Grasof number, elastico-viscous parameter, Lewis parameter, Prandtl parameter, thermophoresis diffusion parameter and Brownian diffusion parameter.

Animasaun et al. [6] treat the Brownian diffusion parameter as dimensionless, while Song et al. [26] and Cao et al. [8] incorporate thermophoresis and random particle motion through the energy and concentration equations. To remove dimensionality from the Brownian diffusion parameter N_b, the concentration difference $\Delta C = (C_w - C_\infty)$ is scaled by the ambient concentration C_∞. Consequently, $N_b = \frac{\varepsilon D_B}{\sigma}\frac{(C_w-C_\infty)}{C_\infty}$ represents a properly normalized, non-dimensional Brownian diffusion parameter.

The transformed boundary conditions are

$f(\zeta) = 0, f'(\zeta) = \gamma f''(\zeta), \theta(\zeta) = 1+\tau\theta'(\zeta), \phi(\zeta) = 1$ at $\zeta = 0$ (11)

$f'(\zeta) = 0, \theta(\zeta) = 0, \phi(\zeta) = 0$ at $\zeta \to \infty$ (12)

where

$\gamma = \frac{L}{\sqrt{\upsilon t\cos\alpha+\frac{\upsilon x}{U_w}\sin\alpha}}$ and $\tau = \frac{D}{\sqrt{\upsilon t\cos\alpha+\frac{\upsilon x}{U_w}\sin\alpha}}$ are momentum and thermal slip factors respectively.

3. Method of Solution

The nonlinear self-similar relations (8) – (12) are transformed into a canonical system of coupled first order ordinary differential equations

$f = y_1, f' = y_2,\ f'' = y_3, f''' = y_4\ , \theta = y_5, \theta' = y_6, \phi = y_7, \phi' = y_8$ (13)

(13) enables the formulation of

$y_1' = y_2, y_2' = y_3, y_3' = y_4, y_5' = y_6, y_7' = y_8$ (14)

Equations (8) – (10) can be re-expressed by invoking the transformations defined in (13) and (14), leading to the following reformulated system:

$$y_4' = \frac{-1}{\frac{\zeta}{2}}\left[\left(y_4\cos\alpha + \left(y_2y_4 + \frac{y_1}{2} - \frac{y_3}{2} + \frac{\zeta}{2}y_3y_4\right)\sin\alpha + \right.\right.$$

$$\left.\left.\frac{1}{k_1\beta}\{(1+\beta)\, y_4 + \frac{\beta}{2}\, y_3(\zeta\cos\alpha + y_1\sin\alpha) - Gry_5 - Gmy_7\}\right. \quad (15)$$

$$y_6' = -[\frac{Pr}{2}\left(\zeta\cos\alpha + y_1\sin\alpha\right) y_6 + N_t y_6^2 + N_b y_6 y_8] \quad (16)$$

$$y_8' = -[\frac{Le}{2}\left(\zeta\cos\alpha + y_1\sin\alpha\right) y_8 + \frac{N_t}{N_b}\, y_6'] \quad (17)$$

The resulting simplified forms of the relevant boundary conditions (12) and (13) are expressed as follows:

$$y_1(0) = 0,\ y_2(0) = \gamma y_3(0),\ y_5(0) = 1+ \tau y_6(0),\ y_7(0) = 1,\ y_8(0) = 0 \quad (18)$$

$$y_2(\infty) = 0,\ y_5(\infty) = 0,\ y_7(\infty) = 0 \quad (19)$$

The coupled boundary-layer equations (15)-(17), subject to the boundary constraints (18)-(19), are numerically integrated using the MATLAB bvp4c solver, enabling accurate computation of solutions over diverse ranges of the controlling flow parameters.

4. Results and Discussion

The non-dimensional governing equations were solved with corresponding boundary conditions by using Matlab solver bvp4c. The solutions and their impact are discussed by considering with fixed fluid flow parameter along with the various elastico-viscous parameter. The fixed parameters and their variation are indicated in the figures. The numerical computations and graphical visualizations were carried out using MATLAB (R2015a), The MathWorks Inc [31].

Accretion at the leading edge is strongly influenced by the inclination angle α. It is prominent for ($0 < \alpha < 180°$), where buoyancy assists the flow, while for ($180° < \alpha < 360°$), the opposing buoyancy force suppresses accretion and will induce flow separation.

Table-I

The values of skin friction coefficient $-f''(0)$, temperature gradient $-\theta'(0)$ and mass transfer rate $-\phi'(0)$ are commuted numerically for different values of moving slot parameter α by setting $k_1 = 0$, with some fixed values of $\beta = Gr = Gm = 0.5$, $N_t = N_b = 0.1$, $Pr = 0.7$, $Le = 2$, $\gamma = 0.2$, $\tau = 0.1$.

$\alpha(Degree)$	$-f''(0)$	$-\theta'(0)$	$-\phi'(0)$
0	1.0293	0.3326	0.6404
25	0.9125	0.3672	0.6881
50	0.8482	0.3863	0.7083
75	0.8080	0.3961	0.7119
100	0.7821	0.3993	0.7030
125	0.7659	0.3972	0.6840

Table-II

The numerically value of temperature gradient $-\theta'(0)$ and mass transfer rate $-\phi'(0)$ are plotted for various values of Prandtl and Lewis number by setting k_1= 0, with fixed values of $\alpha = 125°, \beta$ = 0.5, $Gr = Gm$ = 0, $N_t = N_b$ = 0.1, γ = 0.2, τ = 0.1.

Pr	$-\theta'(0)$	Le	$-\phi'(0)$
$when\ Le = 2$		$When\ \mathrm{Pr} = 0.7$	
0.5	0.2296	0.5	0.0427
1	0.3676	1	0.1731
2	0.6854	2	0.5126
3	1.0048	3	0.8907
4	1.3077	4	1.2781
5	1.5924	5	1.6684
6	1.8599	6	2.0600
7	2.1114	7	2.4523
8	2.3482	8	2.8449
9	2.5713	9	3.2379
10	2.7820	10	3.6310

Velocity Profile: The distributions of the dimensionless velocity $f'(\zeta)$ against ζ illustrated in figs 4.1–4.11 are systematically examined. The velocity profile initially declines and then enhances rapidly but ultimately diminishes with the increase values of Casson fluid Parameter (β), Prandtl number (Pr), Lewis number (Le), thermophoresis diffusion parameter (N_t), Brownian diffusion parameter (N_b), momentum slip factor (γ) and thermal slip factor (τ). However, the velocity rises rapidly and then declining with the increasing influence of slot parameter (α), elastico-viscous parameter (k_1), Grasof number (Gr & Gm). The velocity profile for all the cases are finally settle down at a certain point at $f'(\zeta)$ = 0 when ζ = 8. The velocity of the non-Newtonian Casson fluid in combination with elastico-viscous fluid exhibits a higher peak indicating greater resistance to flow deformation.

From fig: 4.1: An increase in the moving slot parameter α intensifies the suction or injection mechanism at the slot thereby strengthening near wall fluid transport and resulting in a marked enhancement of the velocity field adjacent to the surface.

From figs: 4.2 – 4.3: An increase in the elastico-viscous parameter k_1 strengthens elastic stresses that temporarily store and release deformation energy, effectively

lowering viscous resistance and accelerating the flow. As a result, the velocity rises and the momentum boundary layer thickens, with this enhancement being more pronounced under slip conditions and in Casson fluids, where elastic effects help overcome yield stress. In contrast, the parameter β represents non-Newtonian behavior, higher β intensifies yield stress effects, increases flow resistance and consequently reduces the velocity.

From figs: 4.4 – 4.5: An increase in the Grashof number Gr signifies the prevalence of buoyancy driven thermal effects in the flow regime arising from enhanced temperature gradients which accelerate the fluid motion and strengthen natural convection. Likewise, higher values of the modified Grashof number Gm amplify solutal buoyancy effects, the intensified concentration gradients generate stronger convective forces thereby promoting a further rise in fluid velocity.

From figs: 4.6 – 4.7: An increase in the Prandtl number Pr signifies diminished thermal diffusivity relative to momentum diffusivity causing heat to penetrate the fluid more slowly. Consequently, the thermal boundary layer becomes thinner, convective transport weakens and overall heat transfer efficiency is reduced. Similarly, a larger Lewis number Le implies that thermal diffusion dominates over mass diffusion, this imbalance attenuates concentration gradients, weakens solutal buoyancy forces and thereby suppresses fluid motion and associated convective transport.

From figs: 4.8 – 4.9: As the thermophoresis parameter N_t increases thermally induced migration of suspended particles intensifies promoting enhanced particle transport from hotter to cooler regions. This active particle drift augments momentum exchange within the fluid thereby accelerating the flow and increasing the velocity profile. In contrast, a rise in the Brownian motion parameter $N_b$amplifies random particle agitation which strengthens momentum diffusion and interparticle interactions. The resulting microscopic disorder elevates flow resistance and dissipates kinetic energy, ultimately suppressing the fluid velocity.

From figs: 4.10 – 4.11: As γ increases the fluid experiences less friction at the boundary, allowing it to move more freely. This reduction in boundary resistance leads to a marked escalation in fluid velocity. The thermal slip parameter τ represents the extent to which the temperature at the boundary differs from the temperature in the adjacent fluid layers. Due to the slip condition τ increases, the fluid becomes less heat transfer and weakening the convective forces that drive fluid motion.

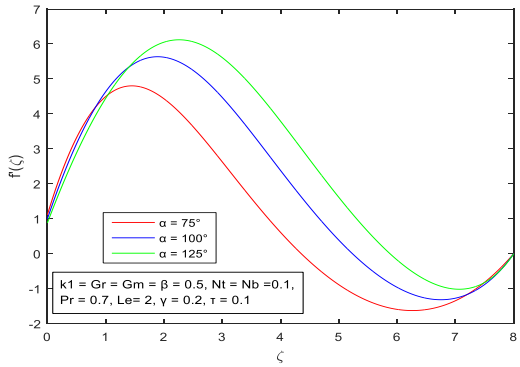

4.1 Velocity Profile with α

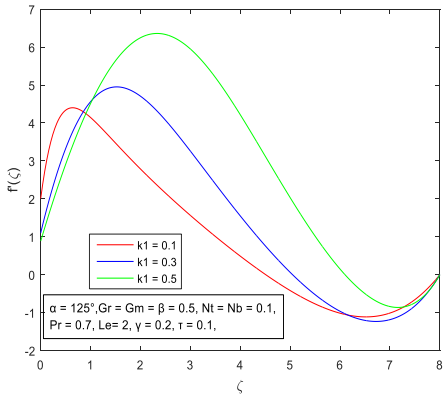

4.2 Velocity Profile with k_1

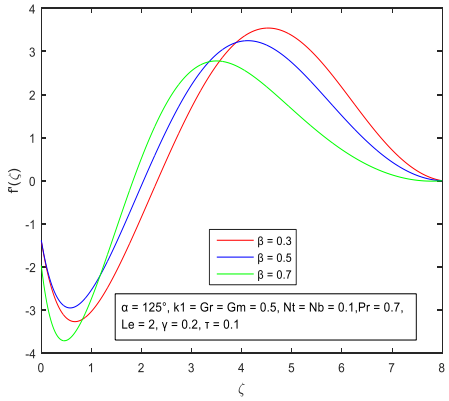

4.3 Velocity Profile with β

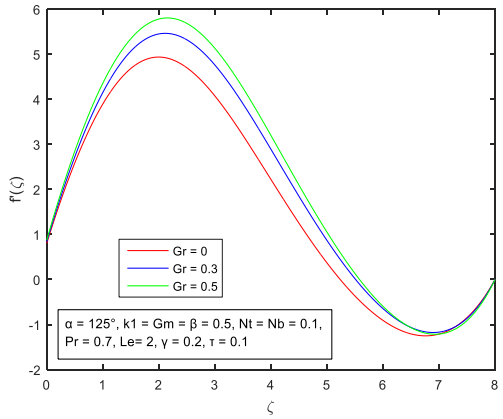

4.4 Velocity Profile with Gr

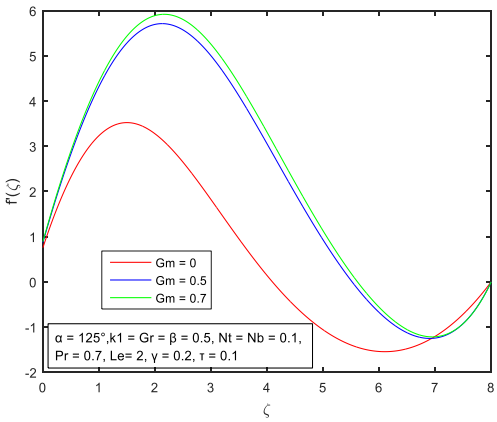

4.5 Velocity Profile with Gm

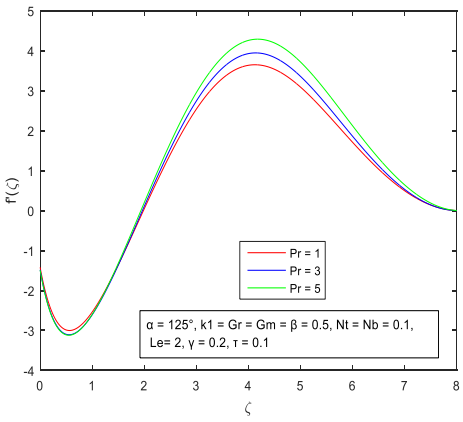

4.6 Velocity Profile with Pr

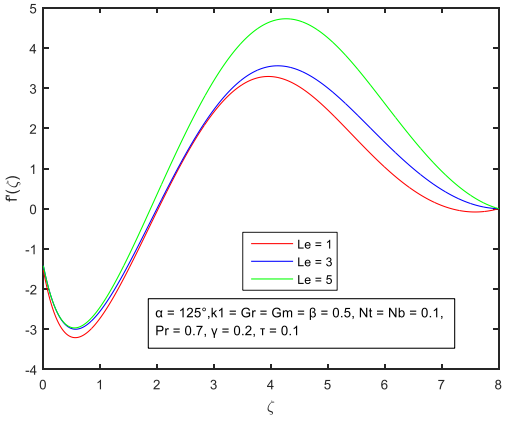

4.7 Velocity Profile with Le

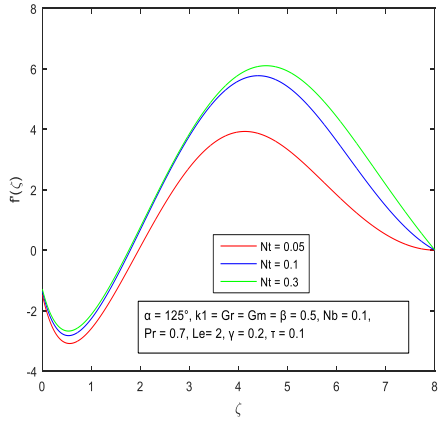

4.8 Velocity Profile with N_t

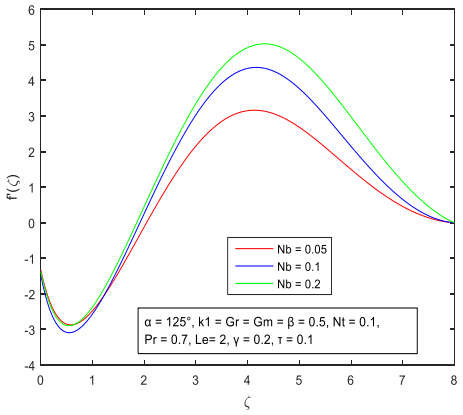

4.9 Velocity Profile with N_b

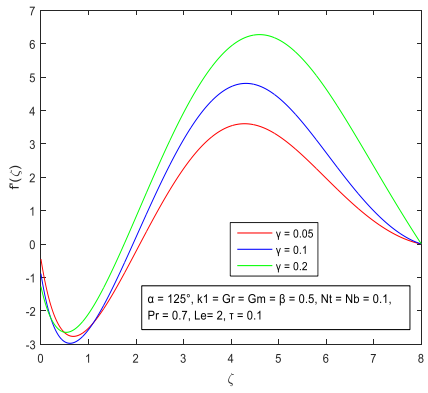

4.10 Velocity Profile with γ

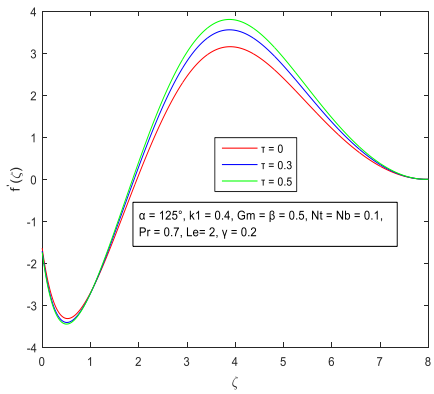

4.11 Velocity Profile with τ

Temperature Profile: The temperature profile $\theta(\zeta)$ against ζ are plotted in figs 4.12 to fig 4.22 are studied. The overall temperature of the fluid decreasing. However, all the fluid layers coincide in terms of temperature means there is no temperature difference between the layers, the condition is called thermal equilibrium in the study with growth of certain fluid flow parameter but ultimately declining after reaching $\theta(\zeta)$ = 1 at ζ = 6 and then temperature slightly rising with the increasing values of slot parameter (α), elastico-viscous parameter (k_1), Casson Fluid Parameter (β), Grasof number (Gr) and thermal slip factor (τ). The temperature of the fluid straight way decreasing in the study of Grasof number (Gm), Prandtl number (Pr), Lewis number (Le), thermophoresis diffusion parameter (N_t), Brownian diffusion parameter (N_b) and momentum slip factor (γ).

From fig: 4.12: With an increase in the slot parameter α, the temperature field of the combined elastico-viscous and Casson fluid becomes progressively more uniform throughout the boundary layer, reflecting enhanced thermal stability of the system. The associated rise in fluid velocity intensifies momentum transport, promotes stronger mixing within the flow domain and consequently augments convective heat transfer.

From figs: 4.13-4.14: An increase in the elastico-viscous parameter k_1 intensifies elastic resistance, suppressing both thermal diffusion and convective transport, which in turn lowers the temperature field and contracts the thermal boundary layer. Likewise, a rise in the Casson fluid parameter β retards the flow velocity, weakening convective heat transfer; the reduced fluid motion limits heat advection, leading to an overall decline in temperature due to less efficient thermal energy redistribution within the fluid.

From figs: 4.15-4.16: As the thermal Grashof number Gr increases, buoyancy forces intensify, strengthening natural convection and accelerating the fluid motion. Similarly, a higher solutal Grashof number Gm amplifies buoyancy effects, producing more vigorous convective transport. The resulting enhancement in convection improves heat transfer efficiency, thereby elevating the fluid temperature through increased thermal energy exchange with the heated surface and the ambient medium.

From figs: 4.17-4.18: A higher Prandtl number Pr corresponds to reduced thermal diffusivity, which confines heat closer to the surface and suppresses its transport into the bulk fluid, thereby lowering the overall temperature field. Similarly, an increase in the Lewis number Le enhances thermal diffusion within the fluid, diminishing heat accumulation near the wall or in localized zones. As a consequence, thermal energy disperses rapidly, reducing temperature levels due to insufficient residence time for effective convective heat transfer.

From figs: 4.19-4.20: An increase in the thermophoretic diffusion parameter N_t strengthens thermophoretic transport, thereby augmenting heat transfer as nanoparticles migrate from high temperature zones and promote stronger particle fluid interactions. In contrast, a rise in the Brownian motion parameter N_b intensifies random molecular diffusion of thermal energy, which weakens convective heat transport. As a result, heat is redistributed more diffusively rather than effectively carried away from the surface, leading to a reduction in the temperature field.

From figs: 4.21-4.22: The momentum slip parameter γ modifies the thermal condition at the solid boundary surface, an increase in γ intensifies the near surface temperature. In contrast, the thermal slip parameter τ governs the wall heat transfer behavior, where elevated τ values weaken the thermal gradient localized adjacent to the bounding surface.

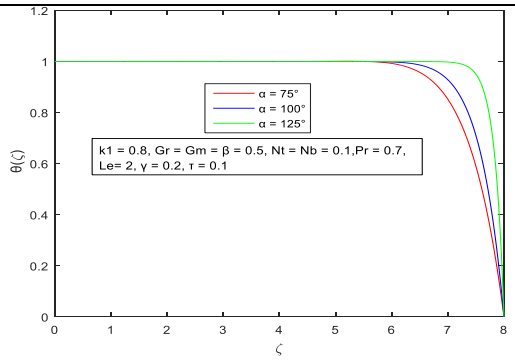

4.12 Temperature Profile with α

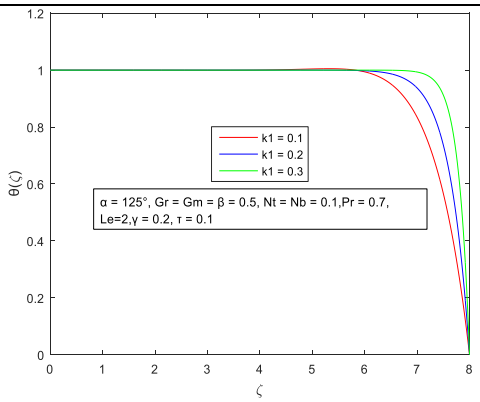

4.13 Temperature Profile with k_1

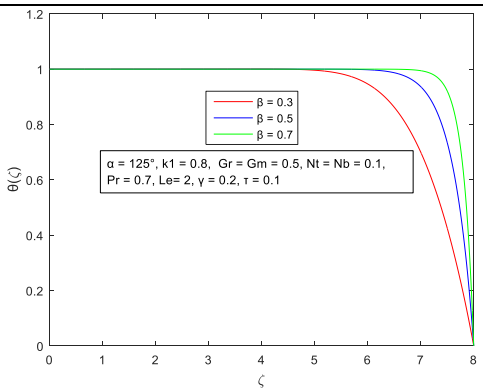

4.14 Temperature Profile with β

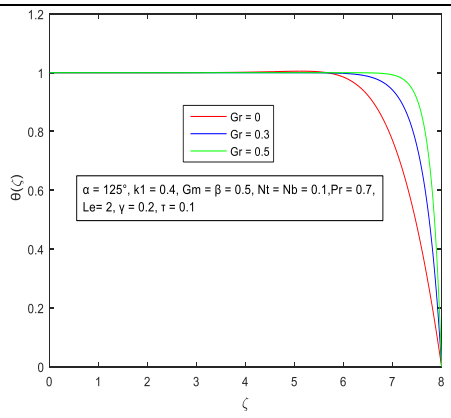

4.15 Temperature Profile with Gr

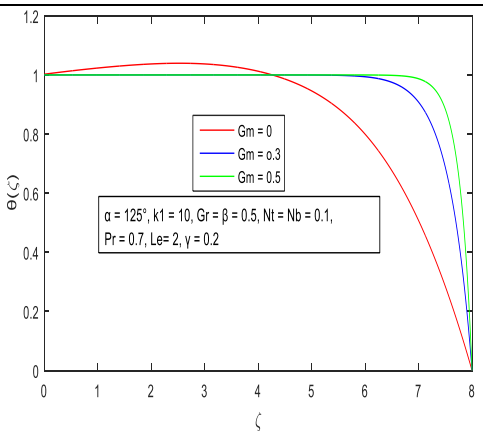

4.16 Temperature Profile with Gm

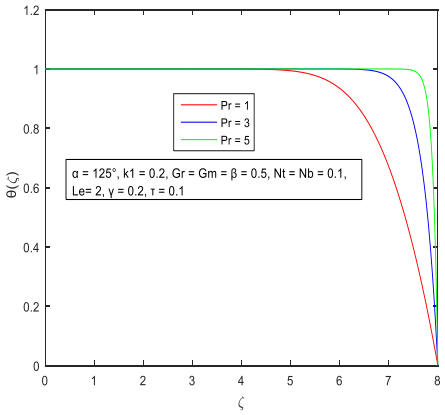

4.17 Temperature Profile with Pr

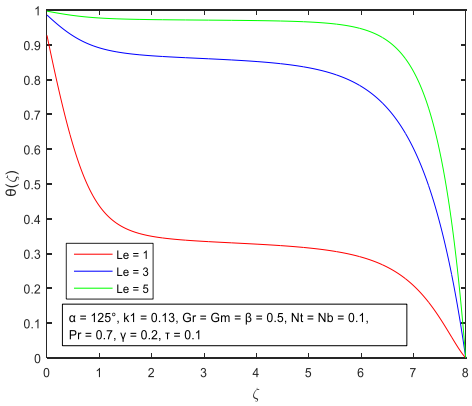

4.18 Temperature Profile with Le

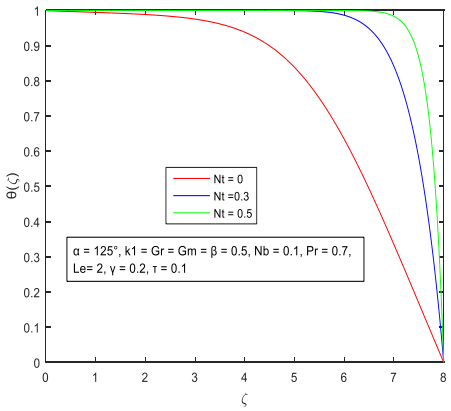

4.19 Temperature Profile with N_t

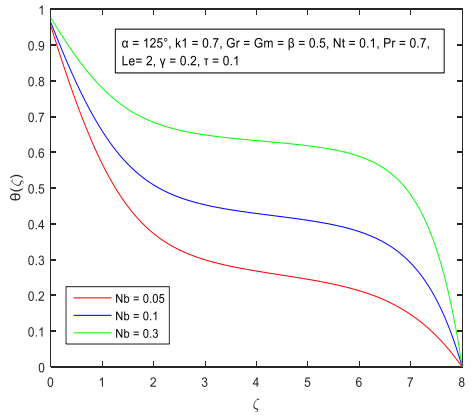

4.20 Temperature Profile with N_b

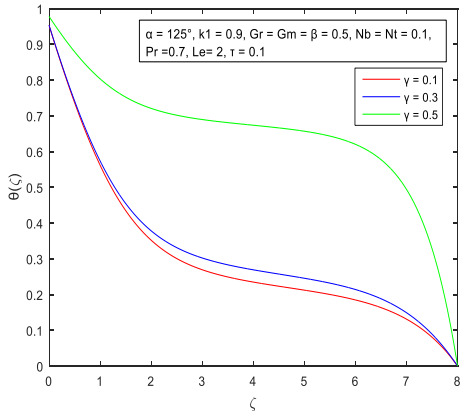

4.21 Temperature Profile with γ

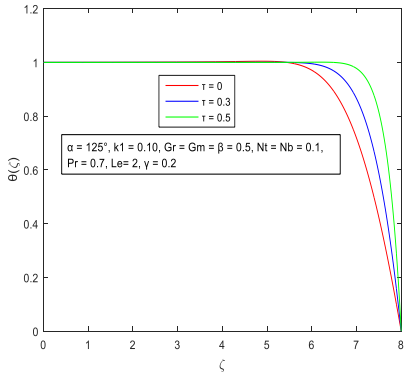

4.22 Temperature Profile with τ

Concentration Profile: The concentration profile $\phi(\zeta)$ against ζ are plotted in figs 4.23 to fig 4.33. The concentration profile overlap at $\phi(\zeta)$ = 1, when ζ = 6 and then start decreasing however with growth of fluid flow parameter such as slot parameter (α), elastico-viscous parameter (k_1), Casson fluid Parameter (β), Grasof number (Gr & Gm), Brownian diffusion parameter (N_b) and thermal slip factor (τ) the concentration distribution slightly increases. The species concentration distribution rapidly decreases but with the rise of Prandtl number (Pr), Lewis number (Le), thermophoresis diffusion parameter (N_t) and momentum slip factor (γ) slightly enhances.

From fig: 4.23: An augmentation in the translational slot parameter α is observed to induce a diminishing trend in the concentration, indicating intensified species diffusion driven by elevated flow velocity. The accelerated motion suppresses the concentration boundary layer thickness, thereby diminishing the accumulation of solute or suspended particles in the vicinity of the surface.

From figs: 4.24-4.25: An increase in the elastico-viscous parameter k_1 strengthens elastic opposition in the fluid, which inhibits molecular diffusion and lowers effective mass transport. Consequently, a distinct spatial profile of species concentration emerges within the flow domain declines and the associated boundary layer thickness contracts. This trend is further accentuated by the Casson fluid β yield stress, slip conditions and leading-edge accretion, all of which impede species diffusion within the boundary layer. Moreover, the accompanying reduction in flow velocity diminishes convective mass transfer, contributing to an overall thickening of the concentration boundary layer.

From figs:4.26-4.27: An increase in the Grashof number Gr, representing intensified convective mass transport, leads to a reduction in the concentration boundary layer thickness adjacent to the surface. Likewise, a higher mass Grashof number Gm strengthens convective motion, promoting more efficient removal of solute species or suspended particles from the boundary region.

From figs:4.28-4.29: Reduced convective velocity weakens thermal transport, thereby intensifying mass diffusion and promoting solute or particle accumulation within the fluid, which may lead to fouling or deposition. An increase in the Lewis number Le signifies lower mass diffusivity, leading to a diminished thickness of the solutal boundary region and reduced near surface concentration. This attenuation of mass diffusion can be either advantageous or adverse, depending on the specific application.

From figs:4.30-4.31: An elevation in the thermophoretic parameter N_t strengthens particle drift from the heated wall toward cooler fluid regions, leading to enhanced particle accumulation away from the surface and a corresponding rise in concentration levels. In contrast, increasing the Brownian motion parameter N_b intensifies stochastic diffusion, producing a more homogeneous concentration distribution within the fluid domain.

From figs:4.32-4.33: As the flow velocity increases, convective mass transfer becomes more dominant, culminating in the attenuation of the solutal boundary layer thickness.

Consequently, solute or particle transport away from the surface is enhanced by the stronger fluid motion. Moreover, higher values of τ are associated with a reduction in the near surface temperature.

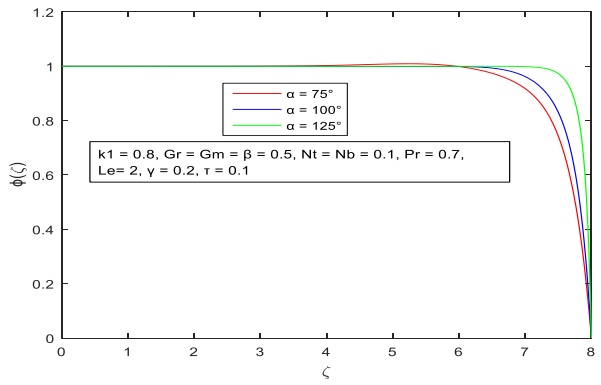

4.23 Concentration Profile with α

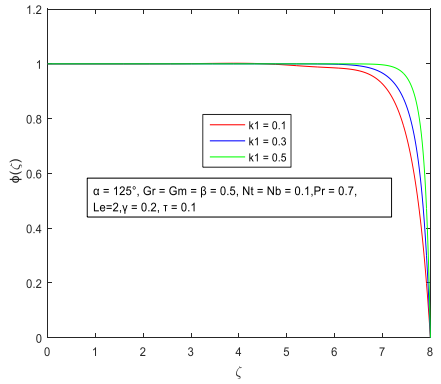

4.24 Concentration Profile with k_1

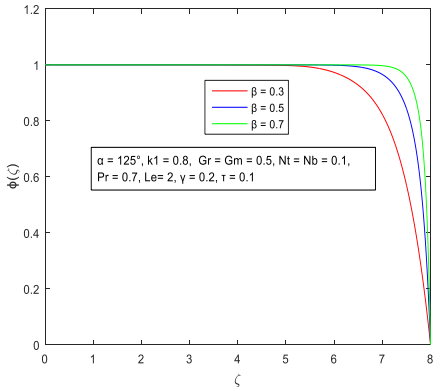

4.25 Concentration Profile with β

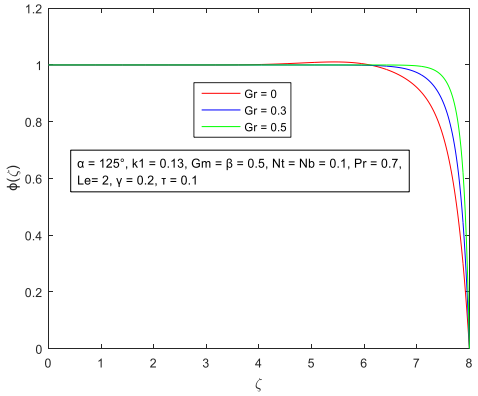

4.26 Concentration Profile with Gr

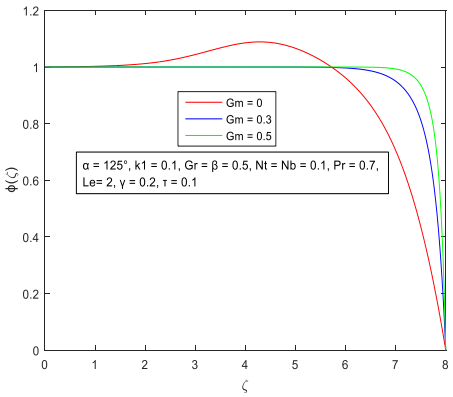

4.27 Concentration Profile with Gm

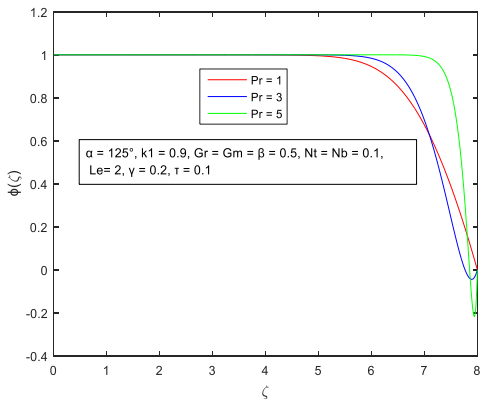

4.28 Concentration Profile with Pr

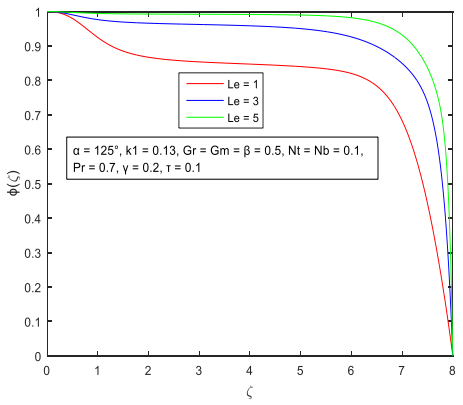

4.29 Concentration Profile with Le

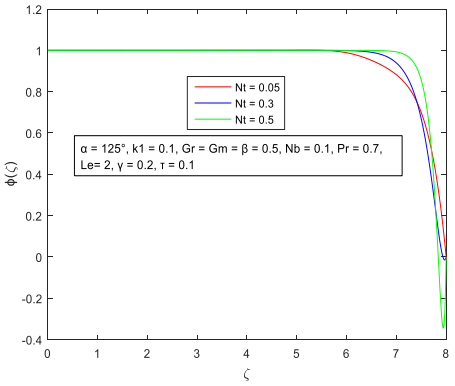

4.30 Concentration Profile with N_t

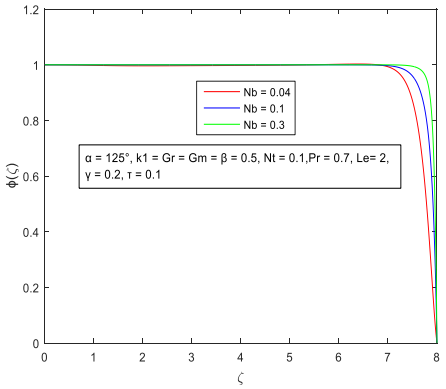

4.31 Concentration Profile with N_b

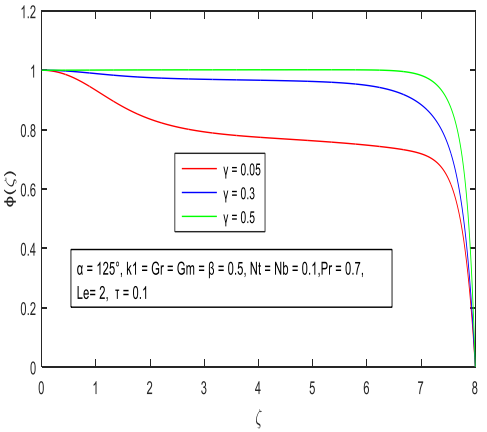

4.32 Concentration Profile with γ

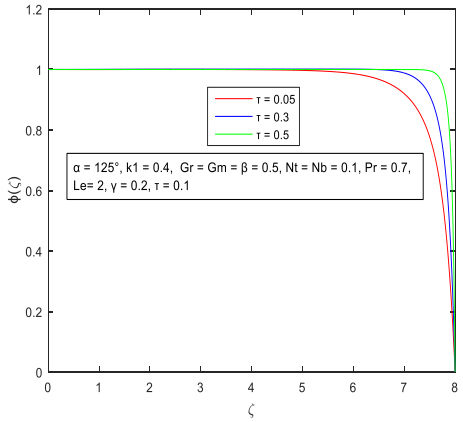

4.33 Concentration Profile with τ

5. Conclusion

In this study the fluid velocity, the fluid temperature and the fluid concentration are completely dominated by the presence of elastico-viscous fluid in combination with Casson fluid and other fluid parameters involved in the flow field. The elastico-viscous fluid significantly effects the flow behaviour of increasing/decreasing velocity, thermal energy and concentration profile of the fluid. The various values of elastico-viscous parameter (k_1) and other fixed values of fluid flow parameter slot parameter (α) = 125°, Casson Fluid Parameter (β) = 0.5, Grashof number of heat transfer and mass transfer (Gr & Gm) = 0.5, Prandtl number (Pr) = 0.7, thermophoresis diffusion parameter (N_t) = 0.1, Brownian diffusion parameter (N_b) = 0.1, Lewis number (Le) =2, momentum slip factor (γ) = 0.2 and thermal slip factor (τ) = 0.1.

The developed model is applicable to non-Newtonian transport phenomena involving coupled momentum, heat, and mass transfer**,** with direct relevance to biomedical systems, microfluidics, thermal engineering, polymer processing, and environmental flows**,** particularly where slip effects, yield stress, and particle dynamics play a dominant role.

The following are the prime factors drawn from this research:

- The fluid velocity is strongly governed by surface motion, elastic effects, buoyancy forces, and slip mechanisms, while it is suppressed by yield stress, thermal diffusion and particle-induced resistance. An increase in the moving slot parameter accelerates the flow by injecting momentum near the wall, similar to blowing air through a narrow slit. Higher elastico-viscous parameter enhances velocity by allowing the fluid to store and release elastic energy, much like a stretched rubber band assisting motion, whereas larger Casson parameter resists flow due to increased yield stress, comparable to pushing toothpaste through a tube. Thermal and solutal buoyancy significantly enhance velocity by natural convection, analogous to hot or salty water rising. In contrast, higher Prandtl and Lewis reduce velocity by limiting thermal and mass diffusion. Thermophoresis promotes motion by driving particles from hot to cold regions, while Brownian motion increases drag and slows the flow. Finally, velocity slip enhances flow by reducing wall friction, whereas thermal slip weakens convective driving forces, leading to reduced fluid motion.
- The elastico-viscous Casson fluid system exhibits enhanced thermal stability due to the combined effects of elasticity, yield stress and buoyancy. Increased fluid motion (via buoyancy parameters) strengthens convection and raises temperature, whereas higher elastico-viscous resistance, Casson parameter, Prandtl number, Lewis number and Brownian motion suppress thermal transport by weakening convection or reducing thermal diffusivity, leading to lower temperature profiles. Thermophoresis enhances heat interaction by driving particles away from hot regions, while surface effects such as momentum and thermal slip modify heat exchange at the wall. Physically**,** this is similar to heating honey mixed with fine particles on a warm plate, stirring (buoyancy) spreads heat efficiently but increasing elasticity or yield stress makes the fluid resist motion, trapping heat near the surface; particles migrating due

to temperature gradients alter heat flow and surface slip changes how easily heat enters or leaves the fluid.

- The concentration boundary layer is strongly governed by the competition between convection, diffusion and elastic–yield effects. An increase in the moving slot parameter and velocity enhances convective transport, thinning the concentration boundary layer and reducing near wall concentration while higher elastico-viscous and Casson effects introduce elastic resistance and yield stress that suppress diffusion and mass transfer. Stronger buoyancy forces promote convective removal of species, further reducing concentration near the surface, whereas reduced velocity or higher Lewis number limits mass diffusivity and allows solute accumulation. Thermophoresis and Brownian motion redistribute particles away from heated regions and promote uniform dispersion. Physically, this behavior is analogous to dye injected into a fast flowing elastico-viscous slurry over a heated plate, higher flow speed and buoyancy rapidly wash the dye away, while elasticity, yield stress, and weaker diffusion allow the dye to accumulate near the surface, potentially causing deposition or fouling.

Nomenclature

Symbol	**Meaning**	**S.I. Unit**
$u(x,y,t)$	Velocity Component of x	(m/s)
$v(x,y,t)$	Velocity Component of y	(m/s)
g	Acceleration due to gravity	(m/s^2)
β_C	Concentration expansion coefficients	(m^3/mol)
β_T	Thermal expansion coefficients	(K^{-1})
C(x,y,t)	Concentration	(mol/m^3)
C_∞	Ambient Concentration	(mol/m^3)
$T(x,y,t)$	Temperature	(K)
T_∞	Ambient temperature	(K)
k_0	Elastico-viscous Parameter	(Pa.s)
D_T	Thermophoresis diffusion coefficient	(m^2/s)
D_B	Brownian diffusion coefficient	(m^2/s)
L	Initial Velocity Slip	-
C_W	Surface concentration	(mol/m^3)
T_W	Surface temperature	(K)

D	Initial Thermal Slip	-
Gr	Thermal Grashof number	-
Gm	Mass Grashof number	-
k_1	Modified Elastico-viscous	(Pa.s)
Pr	Prandtl number	-
Le	Lewis Number	-
N_t	Thermophoresis coefficient	(m/s)
N_b	Brownian diffusion coefficient	(m/s)

Greek Letter

Symbol	**Meaning**	**S.I. Unit**
υ	Kinematic viscosity	Pa.s
μ	Dynamic viscosity	Pa.s
ρ	Fluid density	(Kg/m^3)
ζ	Similarity variable	-
α	Slot Parameter	Radian
β	Casson Fluid Parameter	-
ψ	Stream Function	(m^2/s)
ε	Ratio of heat capacities	-
σ	Thermal diffusivity	(m^2/s)
γ	Momentum Slip Factor	-
τ	Thermal Slip Factor	-
θ	Temperature function	K
$\emptyset$	Concentration function	-

Acknowledgement: The authors are thankful to Referee for valuable comments and suggestions.

References

[1] Adebayo, A.O., Oladimeji, A.A., Peter, A., et al. (2021). Convective flow of nanofluids using Blasius-Rayleigh-Stoke variable with slip effect. *IOSR Journal of Mathematics*, **17**, 1–8.

[2] Al Nuwairan, M. and Souayeh, B. (2021). Blasius Rayleigh Stokes flow over a semi-infinite plate by considering carbon nanotubes. *Microsystem Technologies*, **27**, 2001–2008.

[3] Alammari, M. (2024). Numerical framework of magnetized thermal Casson nanoliquid flow with time-dependent stretching channel enclosing chemical reaction effect and variable fluid properties: A particle swarm optimization with stability. *Modern Physics Letters B*, **38**, 2450109.

[4] Ali, B., Hussain, S., Abdal, S., et al. (2020). Impact of Stefan blowing on thermal radiation and Cattaneo–Christov characteristics for nanofluid flow containing microorganisms with ablation/accretion of leading edge: FEM approach. *European Physical Journal Plus*, **135**, 1–18.

[5] Animasaun, I.L., Kumar, T.K., Noah, F.A., et al. (2023). Insight into Darcy flow of ternary-hybrid nanofluid on horizontal surfaces: Exploration of the effects of convective and unsteady acceleration. *Zeitschrift für Angewandte Mathematik und Mechanik*, **103**, e202200197.

[6] Animasaun, I., Shah, N.A., Wakif, A., et al. (2022). *Ratio of momentum diffusivity to thermal diffusivity: Introduction, metaanalysis, and scrutinization*. Chapman and Hall/CRC.

[7] Asghar, A., Tanveer, S., Govindarajoo, M.V., Ying, T.Y. and Ibrahim, H. (2025). Numerical investigation of MHD Casson hybrid nanofluid flow and heat transfer with permeable stretching/shrinking sheet incorporating porous medium and Joule heating effects. *Journal of Advanced Research in Numerical Heat Transfer*, **38**(1), 48–62.

[8] Cao, W., Animasaun, I., Yook, S.J., et al. (2022). Simulation of the dynamics of colloidal mixture of water with various nanoparticles at different levels of partial slip: Ternary-hybrid nanofluid. *International Communications in Heat and Mass Transfer*, **135**, 106069.

[9] Dianchen Lu, Sumayya Mumtaz, Umer Farooq and Adeel Ahmad (2019). Analysis of unsteady flow and heat transfer of nanofluid using Blasius-Rayleigh-stokes variable. Coatings, **9**, 211.

[10] Eswaramoorthi, S., Nasir, S., Loganathan, K., Gupta, M.S. and Berrouk, A. (2025). Numerical simulation of rotating flow of CNT nanofluids with thermal radiation, ohmic heating, and autocatalytic chemical reactions. *Alexandria Engineering Journal*, **113**, 535–550.

[11] Gangadhar, K., Lakshmi, K.B., Kannan, T., et al. (2022). Stefan blowing on chemically reactive nano-fluid flow containing gyrotactic microorganisms with leading edge accretion (or) ablation and thermal radiation. *Indian Journal of Physics*, **96**, 2827–2840.

[12] Ishaq, A. and Ahmad, A. (2021). Blasius Rayleigh Stokes flow of nanofluid past an isothermal magnetized surface. *Advances in Mechanical Engineering*, 13, 16878140211051818.

[13] Jayaprakash, J. and Govindan, V. (2025). Impact of diffusion and chemical reaction on heat transfer in Casson nanofluids flow over a flat plate with accretion. *Case Studies in Thermal Engineering*, **72**, 106309.

[14] Jayaprakash, J., Govindan, V. and Byeon, H. (2025). Analysis of heat transfer in Casson fluid flow due to aligned flat plate with leading edge accretion and slip boundary conditions. *Advances in Mechanical Engineering*, **17**(4), 1–16. https://doi.org/10.1177/16878132251322300.

[15] Khan M. and Khan W.A. (2016): MHD boundary layer flow of a power-law nanofluid with new mass flux condition – AIP Advances, **6**(2), 025211.

[16] Kumar, K.G., Lokesh, H., Shehzad, S.A., et al. (2020). On analysis of Blasius and Rayleigh Stokes hybrid nanofluid flow under aligned magnetic field. *Journal of Thermal Analysis and Calorimetry*, **139**, 2119–2127.

[17] Mabood, F. and Khan, W.A. (2020). A computational study of unsteady radiative magnetohydrodynamic Blasius and Sakiadis flow with leading-edge accretion (ablation). *Heat Transfer*, *49*, 1355–1373.

[18] MathWorks. (2015). *MATLAB (Version R2015a)*. The MathWorks Inc. https://www.mathworks.com.

[19] Nandi, S., Kumbhakar, B., & Seth, G.S. (2024). Hall and ion slip effects on rotating Casson nanofluid flow past a deformable sheet with multiple slips and activation energy: Modern impressions of non-linear radiation and convection. *International Journal of Applied and Computational Mathematics*, **10**, 65.

[20] Oladapo, O.A., Ajala, O.A., Akindele, A.O., et al. (2024). Effect of radiation on Casson hybrid nano-fluid flow over an inclined surface using Blasius Rayleigh–Stokes variable: Application in solar aircraft. *Engineering Science and Technology*, **5**, 158–179.

[21] Oladimeji, A.A., Ajala, O.A., Adegbite, P. and Ogunsola, A.W. (2021). Convective flow of nanofluids using Blasius-Rayleigh-Stoke variable with slip effect. *IOSR Journal of Mathematics (IOSR-JM)*, **17**(3, Series I), 1–8. https://doi.org/10.9790/5728-1703010108.

[22] Reddy, M.G., Rani, M.S., Kumar, K.G., et al. (2020). Cattaneo–Christov heat flux model on Blasius Rayleigh–Stokes flow through a transitive magnetic field

and Joule heating. *Physica A: Statistical Mechanics and Its Applications*, **548**, 123991.

[23] Saha, B.K. (2026). *Elastico–viscous boundary layer flow over a wedge incorporating nanofluid interaction effects*. *International Journal of Advanced Mathematical Sciences*, **12**(1), 68–78. https://doi.org/10.14419/4bv4wg35.

[24] Shamshuddin, M.D., Mishra, S.R., Anwar Beg, O., Ali Kadir (2018). Numerical study of heat transfer and viscous flow in a dual rotating extendable disk system with a non-Fourier heat flux model. Wiley Periodicals Inc: Heat transfer- Asian Res. 2019; 48:435459 DOI: 10.1002/htj.21392

[25] Sheikholeslami, M., & Ganji, D.D. (2015). Unsteady nanofluid flow and heat transfer in presence of magnetic field considering thermal radiation. *Journal of the Brazilian Society of Mechanical Sciences and Engineering*, **37**(3), 895–902.

[26] Song, Y.Q., Obideyi, B.D., Shah, N.A., et al. (2021). Significance of haphazard motion and thermal migration of alumina and copper nanoparticles across the dynamics of water and ethylene glycol on a convectively heated surface. *Case Studies in Thermal Engineering*, **26**, 101050.

[27] Sravan Kumar T. and Rushi Kumar B. (2017): Unsteady MHD free convective boundary layer flow of a nanofluid past a moving vertical plate. – IOP Conf. Series: Materials Science and Eng., doi:10.1088/1757-899X/263/6/062015

[28] Sravan Kumar, T and Rushi Kumar, B. (2019) Effect of homogeneous-heterogeneous reactions in MHD stagnation point nanofluid flow toward a cylinder with non-uniform heat source or sink. Applied Mathematics and Computing, Trends in Mathematics, https://doi.org/10.1007/978-3-030-01123-9_29

[29] Vaidya, H., Mebarek-Oudina, F., Prasad, K., et al. (2024). Nanofluid flow across a moving plate under Blasius–Rayleigh–Stokes (BRS) variable transport fluid characteristics. *Frontiers in Heat and Mass Transfer*, **22**, 65.

[30] Wang, F., Animasaun, I., Obideyi, B., et al. (2024). Insight into the variations of concentration experiencing leading-edge accretion and thermal analysis: Water conveying nanotubes, graphene, and aluminum oxide nanoparticles over a convectively heated surface. *Journal of Thermal Analysis and Calorimetry*, **149**, 8309–8319.

[31] Yahaya, R. I., Mustafa, M.S., Arifin, N.M., Pop, I., Ali, F.M., & Mohamed Isa, S.S.P. (2025). Heat transfer optimization using RSM for hybrid nanofluid flow impinging obliquely on a permeable shrinking sheet. *Journal of Advanced Research in Numerical Heat Transfer*, **29**(1), 1–15.